Model for Bile Salt Micellization and Solubilization from Studies of a "Polydisperse" Array of Fluorescent Probes and Molecular Modeling

ARTICLE *in* THE JOURNAL OF PHYSICAL CHEMISTRY · DECEMBER 1994

Impact Factor: 2.78 · DOI: 10.1021/j100102a043

2 AUTHORS:

George Li
Memorial Sloan-Kettering Cancer Center
71 PUBLICATIONS **582** CITATIONS
SEE PROFILE

Linda Mcgown
Rensselaer Polytechnic Institute
160 PUBLICATIONS **3,123** CITATIONS
SEE PROFILE

Model for Bile Salt Micellization and Solubilization from Studies of a "Polydisperse" Array of Fluorescent Probes and Molecular Modeling

Guang Li, and Linda B. McGown

J. Phys. Chem., **1994**, 98 (51), 13711-13719 • DOI: 10.1021/j100102a043

Model for Bile Salt Micellization and Solubilization from Studies of a "Polydisperse" Array of Fluorescent Probes and Molecular Modeling

Guang Li and Linda B. McGown*

Department of Chemistry, P. M. Gross Chemical Laboratory, Duke University, Box 90346, Durham, North Carolina 27708-0346

Received: August 10, 1994; In Final Form: October 13, 1994[⊗]

The micellar aggregation of the bile salt sodium taurocholate (NaTC) in water, in the concentration range 0−35 mM, was studied by using a "polydisperse" array of polycyclic aromatic hydrocarbon probes, ranging from pyrene with four aromatic rings to ovalene with 10 aromatic rings. Measurements of fluorescence spectra, peak intensity, vibronic band intensity ratio, and lifetime were used to follow the solubilization of the probes as a function of NaTC concentration. The results strongly support stepwise aggregation behavior since at least two critical regions of NaTC concentration were reported by each of the probes. For all probes, one of these critical regions occurs at 8−12 mM. The other critical concentration regions, referred to as "apparent critical micellar concentrations" (acmc), increase with increasing probe size and include 4, 15, and 20 mM. Molecular modeling was used to develop a model for micellar aggregation and probe solubilization for NaTC in water that incorporates experimental results of this and previous studies as well as considerations of molecular dimensions and aggregate conformational energy in the absence of solvent.

Introduction

Bile salt micelles have been extensively studied because of interest in their biological functions and, more recently, their applications in analytical chemistry.[1−4] However, fundamental studies of their aggregation behavior remain necessary until an aggregation model that is consistent with the various experimental results and which can resolve various points of controversy can be established.[4−12] An accurate model for aggregation of bile salts is essential in order to understand their role in biological processes and for their further application in chemical separations and measurements.

One aggregation model for bile salts is the primary−secondary micelle model,[5,6] which involves a stepwise aggregation mechanism in which a primary micellar unit undergoes secondary aggregation to form larger micellar aggregates in a polydisperse, concentration-dependent system. The model was developed using a simple "CPK" (or space filling) molecular modeling and was supported by some experimental evidence;[1,5] quasi-elastic light-scattering experiments indicated some 20−45% variation around the average aggregate size.[6] Although some other models were proposed as well,[7,8] this model has still been used in recent work. The stepwise nature of bile salt aggregation was also indicated by light-scattering experiments[2,9] which identified three transition "limits", each attributed to a new form of aggregate.

Stepwise aggregation and polydispersity of sodium taurocholate (NaTC), which is a trihydroxy bile salt, were supported by studies of critical micelle concentration (cmc). The results indicated a broad, "quasi-cmc" around 8−12 mM[11] that was even considered by some to be too broad to be a cmc.[12,13] According to a recent development on the theoretical interpretation of cmc broadening phenomena, a broad critical region is evidence of the polydispersity of the micellar solutions.[14,15] A study of the solubilization of naphthalene by the trihydroxy bile salt sodium cholate (NaC) indicated the presence of more than one cmc, again suggesting polydispersity of bile salt micelles.[13] By fitting the experimental data with assumed aggregation models, a dimer−oligomer model was proposed since the fitting was successful with the polydisperse aggregation model but failed with any monodisperse model.

Evidence for stepwise aggregation and polydispersity of bile salt solutions has also been provided by fluorescence probe studies, which identified two critical regions in NaTC aggregation.[10,11,16] The first critical region is at 3−5 mM and may be the region at which dimers begin to form, as indicated by fluorescence changes in some smaller polycyclic aromatic hydrocarbon (PAH) probes. The second critical region occurs over a broad concentration range around 8−12 mM, at which the PAH probes begin to be solubilized in relatively apolar environments, signaling the formation of larger aggregates of NaTC that are capable of isolating the probes in interior binding sites that afford protection from the bulk solution.

In a recent study of NaTC and its dihydroxy analogue sodium taurodeoxycholate in water, dynamic measurements of fluorescence anisotropy decay of perylene successfully resolved the bile salt dimers from larger aggregates and quantitatively reported the mole fraction of dimer, i.e., the moles of dimer divided by the total moles of aggregates.[16] Although quantitative information on the distribution of larger aggregates could not be obtained by this technique, the work suggested stepwise aggregation for NaTC based on the change in the dimer molar fraction and suggested that different sizes of aggregates form at different "cmc's".

Key to the success of the anisotropy studies was the ability of the bile salt dimers to solubilize the perylene probe. However, it is obvious that the bile salt dimer is not large enough to solubilize PAHs of all sizes and that larger PAH probes require larger bile salt aggregates. Therefore, it is expected that the use of a range of probe sizes could provide a more accurate and detailed view of the concentration dependence of bile salt aggregate size and polydispersity, since transitions in the fluorescence properties of the probes would indicate critical regions for the formation of different sizes of bile salt aggregates. This is the basis of the present work, in which a "polydisperse" array of PAH probes was used to sense the formation of different sizes of NaTC aggregates. Five PAHs, in which the largest

[⊗] Abstract published in *Advance ACS Abstracts,* November 15, 1994.

0022-3654/94/2098-13711$04.50/0

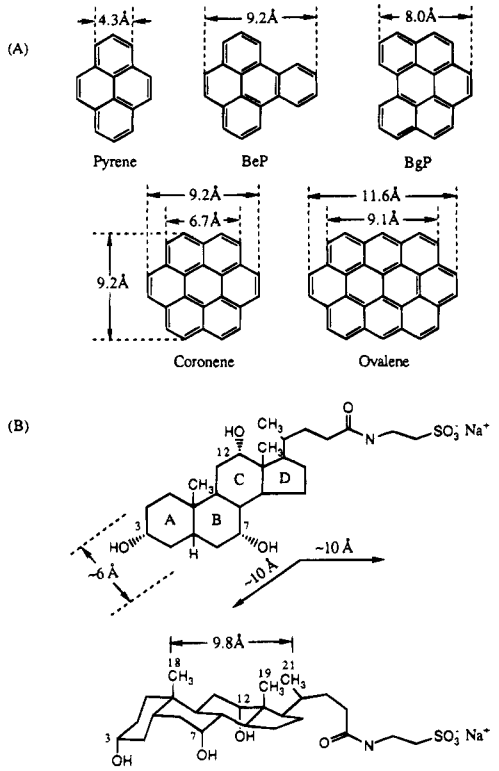

Figure 1. Molecular structures of (A) polycyclic aromatic hydrocarbon (PAH) probes and (B) sodium taurocholate (NaTC). Hydrogen atoms on the aromatic rings and saturated rings are included in the dimensions.

(ovalene) has more than twice the surface area as the smallest (pyrene), comprised the array. Their structures are shown in Figure 1. The experimental results are combined with molecular modeling calculations to formulate a model for NaTC aggregation and probe solubilization in water.

Experimental Section

Materials. Sodium taurocholate (NaTC, Ultrol grade, >98%, Calbiochem), pyrene (99%, Aldrich), benzo[*e*]pyrene (BeP, 99%, Aldrich), benzo[*g,h,i*]perylene (BgP, 99%, AccuStandard), and coronene (99%, Aldrich) were all used as received. Ovalene was synthesized and provided by Dr. J. C. Fetzer[17] and used without further purification. Stock solutions of the PAH probes were prepared in absolute ethanol with the exception of ovalene, which was prepared in 1:1 (v/v) mixture of methylene chloride and methanol.

For preparation of the solutions of the probes in NaTC, appropriate amounts of the stock solutions of the probes were added to 5.0 mL volumetric flasks, and the solvent was evaporated by a gentle flute of N_2. The aqueous NaTC solutions were then prepared directly in the volumetrics with HPLC-grade water. The probe concentration in the NaTC solutions was 2.0 μM unless otherwise indicated. All of the solutions were sonicated for at least 1.5 h (2 h for ovalene) to maximize the solubilization of the PAH probes. The solutions were then allowed to equilibrate overnight prior to measurement. Stable, reproducible measurements were taken as an indication of adequate equilibration.

Measurements. Fluorescence lifetimes were measured using a multiharmonic Fourier transform phase-modulation fluorometer (Model MHF, SLM Instruments, Inc.). A HeCd laser (LiCONiX) was used to provide exciting light at 325 nm for all of the probes except ovalene, for which the 442 nm line was used. The emission beam was passed through a bandpass optical filter (10 nm width) centered at 400 nm for pyrene, 400 or 420 nm for BeP, 420 or 470 nm for BgP, and 440 or 470 nm for coronene. Ovalene emission was measured through a wider emission window created by the combination of a long-pass filter at 470 nm and a short-pass filter at 560 nm, in order to obtain sufficient intensity for the measurements. A polarizer in the excitation beam was set to pass vertically polarized light and one in the emission beam was set to the magic angle (54.7°) in order to eliminate photoselection effects. The temperature of the sample chamber was maintained at 20.0 ± 0.1 °C.

Scattered light was used as the lifetime reference. Fifteen pairs of sample−reference measurements were made, in which each measurement is the average of 100 samplings over a period of 24 s, performed internally by the instrument. For each probe, data at 10−20 modulation frequencies in the range 5−100 MHz were selected to optimize the frequency range and provide a good signal-to-noise ratio. The acquired standard deviations of phase angle difference (PAD) and modulation amplitude ratio (MAR) were calculated and used in the nonlinear least-squares minimization algorithm as the "error" term in the expression of reduced χ^2. Global analysis software (Version 3, Globals Unlimited) was used to analyze the lifetime data. Uncertainties in the fitted values were estimated by the software. The best fitting was judged not only by the reduced χ^2 value but also by the randomness of the fitting residuals of both PAD and MAR.

Excitation and emission spectra were collected on a multifrequency phase-modulation spectrofluorometer (Model 48000S, SLM Instruments, Inc.) using 1 nm scanning intervals for all probes except ovalene, for which 2 nm steps were used. The sample chamber temperature was maintained at 20.0 ± 0.1 °C.

Light scattering measurements were performed on the 48000S instrument with the same 90° configuration that was used for the fluorescence measurements. Excitation and emission wavelengths were both set to 500 nm, at which there is no sample absorption, with bandwidths of 2 nm. Each scattered light intensity is the average of seven replicate measurements for each of three individual solutions at each NaTC concentration. Filtering the solutions prior to measurement with a 0.22 μm filter decreased the scattered light intensities slightly but the trends were the same as for the nonfiltered samples. The results reported here were obtained for the nonfiltered solutions.

Molecular Modeling. Molecular modeling software (SYBYL Version 6.0, TRIPOS) was implemented on a SUN SPARC Station 2 (Sun Microsystems, Inc.) to optimize the conformation of the NaTC aggregates in the absence and presence of probes. In SYBYL, the Gasteiger−Hückel method was used to calculate the net charges of the atoms in both nonaromatic and aromatic molecules (or molecular groups). The TRIPOS all-atom potential function was used to evaluate the intermolecular and intramolecular interaction energies of the aggregates and aggregate−probe complexes in the energy refining (minimization) process. The total energy difference between an optimized aggregate/complex conformation and the sum of the individual components (NaTC monomers, probe) was calculated and used to judge the relative stability of the possible conformations. Unless otherwise mentioned, solvent molecules were not included and the dielectric constant was assigned a value of 1.0. This value was used in order to identify the most stable aggregate conformations based on the structures of the NaTC monomer and probe molecules. Possible effects of the aqueous solvent on the aggregate structures are discussed below.

Results and Discussion

Steady-State Fluorescence Results. *Fluorescence Spectra.* Fluorescence excitation and emission spectra of the probes in aqueous solutions containing various concentrations of NaTC were collected. The emission spectra are shown in Figure 2. For all of the probes except pyrene, which has a relatively high

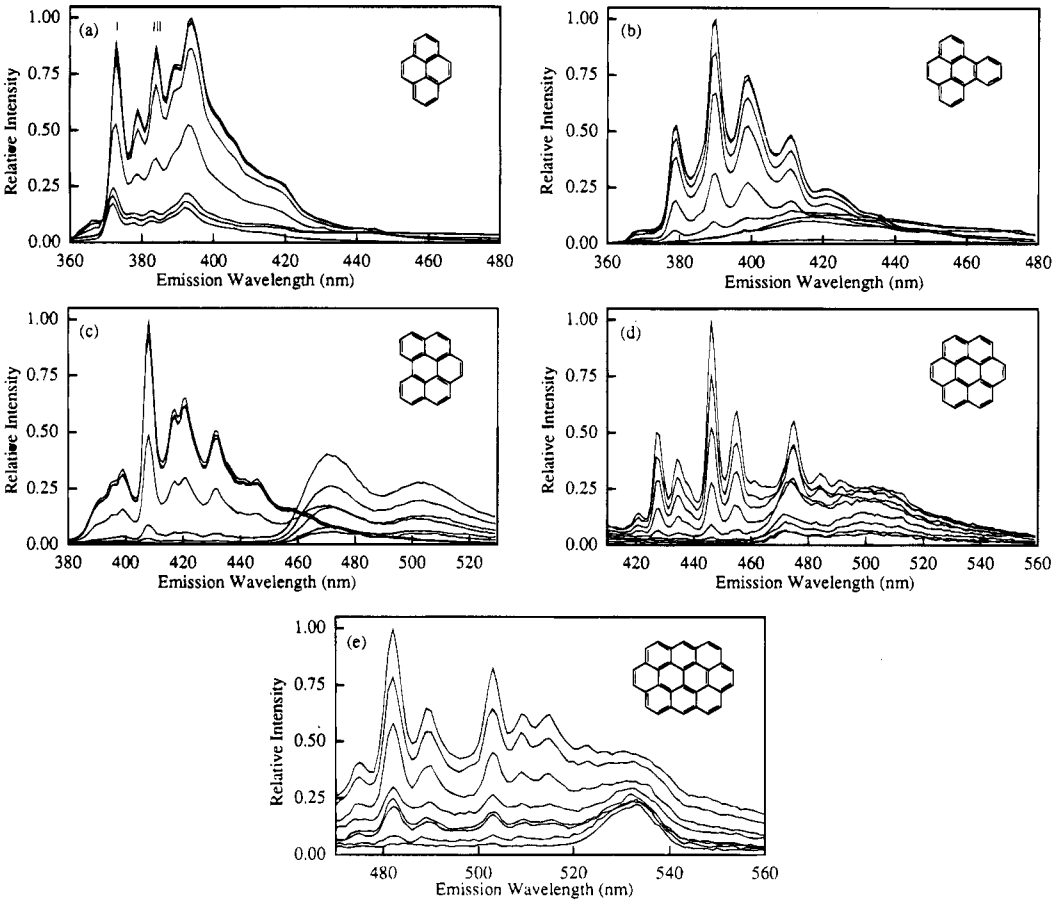

Figure 2. Fluorescence emission spectra of the PAH probes (2 μM) in water (except ovalene) and in aqueous solutions of NaTC at concentrations of 0, 4.0, 8.0, 12.0, 15.0, 20.0, 25.0, 30.0, and 35.0 mM. (a) Pyrene, (b) BeP, (c) BgP, (d) coronene, (e) ovalene. The excitation wavelength for (a)−(d) is 325 nm and for (e) is 442 nm. For all probes, the molecular peak intensities increase with increasing NaTC concentration.

aqueous solubility (0.4−0.7 μM),[18] there is a minimum NaTC concentration below which there is no emission from individually solubilized probe molecules. However, the broad, featureless emission spectra to the red of the molecular peaks at low NaTC concentrations and even in pure water indicate the presence of probe aggregates (e.g., microcrystals, oligomers, dimers) in the bulk solution. The appearance of both probe aggregates and solubilized probe molecules was further evidenced by differences between the excitation spectra measured at the molecular emission peaks and those measured at the broad emission peaks. This is consistent with previous observations of probe aggregates in aqueous solution.[19,20]

The different probes exhibit different distributions between their molecular and aggregate peaks as a function of NaTC concentration. Pyrene exhibits a very weak aggregate peak that is probably due to pyrene dimer or excimer. BeP and BgP exhibit significant aggregate peaks that decrease in intensity at high NaTC concentrations—the transition from an aggregate spectrum to a molecular spectrum is particularly striking for BgP. For coronene and ovalene, the two largest probes, the aggregate peak is present at all NaTC concentrations. The apparent increase in intensity of the aggregate peaks may be due to increased solubilization of aggregates in the presence of bile salt as well as superimposition of the aggregate peak on the increasing molecular peaks.

Fluorescence Intensity. Relative fluorescence intensity of the molecular peaks of the probes as a function of NaTC concentration is shown in Figure 3. Fluorescence enhancements with increasing NaTC concentration are seen for all of the probes within the NaTC concentration range studied. The fluorescence intensity for each probe is normalized in Figure 3 to a maximum

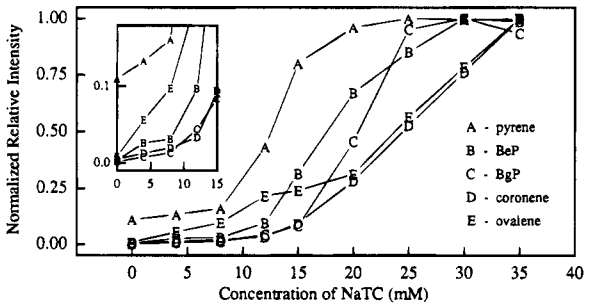

Figure 3. Normalized relative fluorescence intensity of the PAH probes vs NaTC concentration. Inset: expanded intensity axis for the 0−15.0 mM NaTC region.

value of unity, so comparison of intensity cannot be made between different probes.

The curves in Figure 3 show several different critical concentration regions, including the primary critical region at 8−12 mM for all probes as well as secondary critical regions at 15 mM for BgP and coronene and 20 mM for ovalene. Thus, all of the probes show the previously reported transition around 8−12 mM NaTC, but some also show other critical regions that range from 4 to 20 mM. A secondary critical region indicated by the fluorescent probes is referred to hereinafter as an "apparent cmc" (acmc).

The results shown in Figure 3 are all for probe concentrations of 2 μM. The same experiment was also performed using 1 μM coronene, and the plot was identical to that for 2 μM coronene shown in Figure 3. The similarity between the two curves indicates that the acmc's are independent of probe concentration in this concentration range.

For the three smaller PAHs (pyrene, BeP, and BgP) fluores-

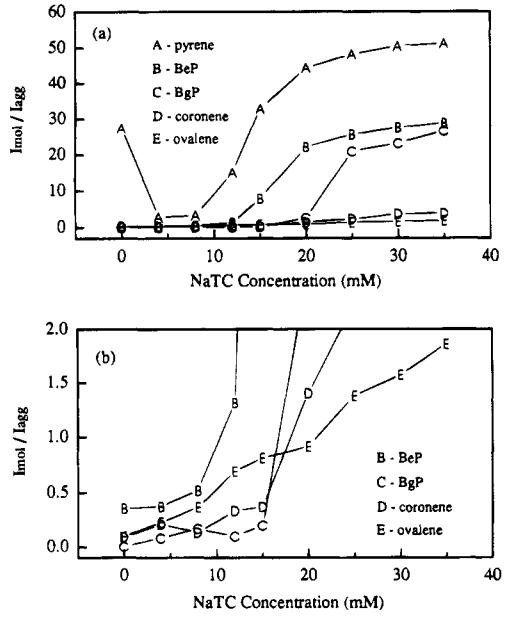

Figure 4. Ratio of the fluorescence intensity of a molecular peak (I_{mol}) to the intensity of the probe aggregate peak (I_{agg}), measured at the following emission wavelengths ($\lambda_{em,mol}/\lambda_{em,agg}$): pyrene, 384 nm/460 nm, BeP, 390 nm/460 nm, BgP, 421 nm/500 nm, coronene, 446 nm/500 nm, ovalene, 503 nm/533 nm. (a) Full scale data for all probes. (b) Data for all probes except pyrene plotted on an expanded intensity axis.

cence intensity at the molecular peak levels off and the probe aggregate peak disappears before the highest NaTC concentration of 35 mM has been reached, indicating that complete solubilization of the probe has been achieved. For the two larger PAHs (coronene and ovalene), the molecular peak intensity does not level off, nor is the aggregate peak substantially diminished, within the concentration range shown in Figure 3.

Intensity Ratios of Molecular to Aggregate Peaks and of Molecular Vibronic Bands. Figure 4 shows the ratio of the intensity of a vibronic band corresponding to an allowed transition in the molecular spectrum to the intensity of the aggregate peak for each of the probes as a function of NaTC concentration. The primary critical region at 8−12 mM and acmc regions indicated by these plots are similar to those indicated by Figure 3, with the addition of an acmc around 4 mM for pyrene which is consistent with previous reports.[10,11]

For PAH compounds that have D_{2h} symmetry, the fluorescence intensities of different vibronic bands show different solvent dependencies, depending on whether the corresponding transition is allowed or forbidden. Thus, the intensity ratio of a "forbidden" vibronic band to an "allowed" vibronic band serves as a measure of the microenvironmental polarity experienced by the molecule.[21−23] This phenomenon is known as the Ham effect.

Vibronic band intensity ratio (VBIR) values vs NaTC concentration were determined from the spectra in Figure 2 for pyrene (Figure 5), which is a good Ham effect probe and is sufficiently soluble in water to provide a range of VBIR as NaTC concentration is increased from 0 to 35 mM. The results indicate that pyrene experiences increasingly apolar microenvironments as NaTC concentration is increased above 4 mM, which was identified above as the acmc of pyrene. There is a change in slope at 8 mM, corresponding to the primary critical region and suggesting the formation of different NaTC aggregates above this concentration. The gradual increase in VBIR as a function of NaTC concentration is consistent with previous work.[10]

For the other probes, VBIRs were also determined from the spectra in Figure 2 at concentrations above the critical 8−12 mM region only, due to the absence of solubilized monomer at lower concentrations. In all cases, the VBIR gradually decreases as NaTC concentration increases, with no breaking points in the curves. This indicates a gradual increase in the average aggregate size, resulting in increasingly hydrophobic, apolar binding sites that are better protected from the bulk solution.

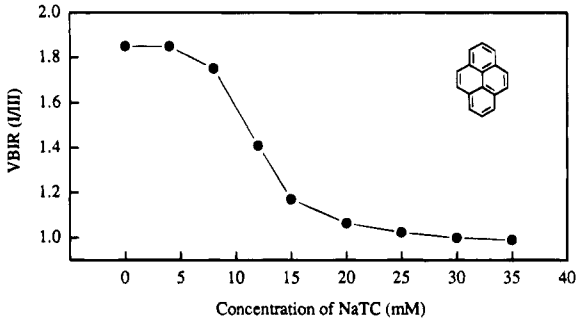

Figure 5. Vibronic band intensity ratio vs NaTC concentration for pyrene.

TABLE 1: Fluorescence Lifetimes (τ) and Fractional Intensity Contributions (f) of Pyrene (2.0 μM) in Aqueous NaTC Solutions (λ_{em} = 400 nm)

C_{NaTC}, mM	f_1	τ_1, ns	f_2	τ_2, ns	χ_R^2
0	0.910 ± 0.002	138 ± 1	0.090	15.0 ± 0.4	0.10
4.0	0.914 ± 0.003	139 ± 3	0.086	14.1 ± 0.7	0.47
8.0	0.925 ± 0.001	161 ± 3	0.075	14.8 ± 0.7	0.58
12.0	0.988 ± 0.001	228 ± 2	0.012	11.3 ± 1.1	0.14
15.0	0.993 ± 0.001	278 ± 2	0.007	9.6 ± 1.2	0.21
20.0	0.994 ± 0.001	326 ± 2	0.006	9.7 ± 1.5	0.34
25.0	0.994 ± 0.001	336 ± 2	0.006	8.9 ± 1.3	0.30
30.0	0.994 ± 0.001	343 ± 3	0.006	8.0 ± 1.3	0.31
35.0	0.993 ± 0.001	350 ± 4	0.007	8.5 ± 1.5	0.54

TABLE 2: Fluorescence Lifetimes (τ) and Fractional Intensity Contributions (f) of BeP (2.0 μM) in Aqueous NaTC Solutions

λ_{em}, nm	C_{NaTC}, mM	f_1	τ_1, ns	f_2	τ_2, ns	χ_R^2
400[a]	4.0	0.788 ± 0.004	19.2 ± 0.2	0.212	5.7 ± 0.1	0.09
	8.0	0.710 ± 0.009	21.0 ± 0.4	0.290	5.4 ± 0.2	0.57
	12.0	0.727 ± 0.009	38.8 ± 1.1	0.273	7.7 ± 0.3	0.62
	15.0	0.920 ± 0.002	54.1 ± 0.6	0.080	7.3 ± 0.3	0.82
	20.0	0.975 ± 0.002	56.9 ± 0.3	0.025	4.7 ± 0.5	0.60
	25.0	0.978 ± 0.002	58.0 ± 0.3	0.022	4.6 ± 0.5	0.63
	30.0	0.980 ± 0.002	58.4 ± 0.3	0.020	4.0 ± 0.4	0.67
	35.0	0.974 ± 0.002	58.2 ± 0.4	0.026	4.7 ± 0.4	0.74
420	0			1.000	19.0 ± 0.3	1.55
	4.0			1.000	18.2 ± 0.6	1.67
	8.0[b]			1.000	16.8 ± 0.4	1.34
		0.217 ± 0.021	35.4 ± 5.0	0.783	14.6 ± 0.2	0.60
	12.0	0.262 ± 0.020	47.2 ± 5.8	0.738	17.1 ± 0.3	0.76
	15.0	0.718 ± 0.005	50.7 ± 0.7	0.282	14.1 ± 0.2	0.34
	20.0	0.952 ± 0.003	55.2 ± 0.5	0.048	5.4 ± 0.4	0.62
	25.0	0.964 ± 0.003	57.8 ± 0.5	0.036	4.6 ± 0.4	0.70
	30.0	0.968 ± 0.002	58.5 ± 0.5	0.032	3.4 ± 0.3	0.87
	35.0	0.962 ± 0.002	58.7 ± 0.6	0.038	3.7 ± 0.3	0.65

[a] At C_{NaTC} = 0 mM, lifetime data are not available because of low fluorescence intensity. [b] Both one-component and two-component fits are shown.

Fluorescence Lifetime Studies. *Fluorescence Lifetime Results.* Fluorescence lifetime measurements of the probes as a function of NaTC concentration are useful not only to probe the aggregation behavior of the bile salt but also to monitor the solubilization of the probes. Fluorescence lifetime results for the five probes are shown in Tables 1−5. The lifetimes were measured for BeP, BgP, and coronene at two emission wavelengths: one on a molecular peak and one on a probe aggregate peak. Lifetimes were measured only at a molecular peak for pyrene because the aggregate peak was too weak. For ovalene,

TABLE 3: Fluorescence Lifetimes (τ) and Fractional Intensity Contributions (f) of BgP (2.0 μM) in Aqueous NaTC Solutions

λ_{em}, nm	C_{NaTC}, mM	f_1	τ_1, ns	f_2	τ_2, ns	f_3	τ_3, ns	χ_R^2
420[a]	4.0	0.581 ± 0.031	15 ± 2	0.419	1.6 ± 0.3			0.36
	8.0	0.638 ± 0.023	12 ± 1	0.362	1.4 ± 0.2			0.27
	12.0	0.610 ± 0.027	58 ± 11	0.390	3.2 ± 0.4			0.82
	15.0	0.808 ± 0.008	81 ± 4	0.192	3.1 ± 0.3			1.22
	20.0	0.956 ± 0.003	97 ± 1	0.044	3.7 ± 0.4			0.44
	25.0	0.973 ± 0.002	97 ± 1	0.027	2.9 ± 0.6			0.81
	30.0	0.968 ± 0.002	99 ± 1	0.032	3.8 ± 0.4			0.39
	35.0	0.964 ± 0.002	99 ± 1	0.036	3.8 ± 0.4			0.51
470	0	0.379 ± 0.006	9.5 ± 0.2	0.621	2.89 ± 0.03			0.24
	4.0	0.315 ± 0.006	9.6 ± 0.2	0.685	2.71 ± 0.02			0.11
	8.0	0.333 ± 0.007	10.1 ± 0.3	0.667	2.71 ± 0.03			0.14
	12.0	0.329 ± 0.002	11.4 ± 0.6	0.671	2.60 ± 0.02			0.81
	15.0	0.257 ± 0.006	10.1 ± 0.3	0.743	2.97 ± 0.02			0.88
	20.0[b]	0.317 ± 0.005	54 ± 5	0.683	3.00 ± 0.04			1.93
		0.256 ± 0.004	79 ± 4	0.244[c]	6.9 ± 0.1	0.500	2.4 ± 0.1	0.38
	25.0	0.841 ± 0.004	97 ± 2	0.085[c]	7.3 ± 0.5	0.074	2.0 ± 0.2	0.29
	30.0	0.859 ± 0.004	99 ± 2	0.081[c]	5.6 ± 0.5	0.060	2.1 ± 0.2	0.47
	35.0	0.874 ± 0.005	98 ± 2	0.073[c]	6.5 ± 0.5	0.053	2.0 ± 0.3	0.65

[a] At C_{NaTC} = 0 mM, lifetime data are not available because of low fluorescence intensity. [b] Both two-component and three-component fits are shown. [c] The standard deviation for f_2 is the same as that for f_1.

TABLE 4: Fluorescence Lifetimes (τ) and Fractional Intensity Contributions (f) of Coronene (2.0 μM) in Aqueous NaTC Solutions

λ_{em}, nm	C_{NaTC}, mM	f_1	τ_1, ns	f_2	τ_2, ns	f_3	τ_3, ns	χ_R^2
440[a]	8.0	0.075 ± 0.012	101 ± 76	0.582 ± 0.019	8.5 ± 0.4	0.343	1.0 ± 0.2	0.09
	12.0	0.293 ± 0.010	129 ± 43	0.404 ± 0.015	7.6 ± 0.4	0.303	1.3 ± 0.1	0.10
	15.0	0.462 ± 0.009	175 ± 19	0.341 ± 0.009	8.7 ± 0.3	0.197	1.5 ± 0.1	0.33
	20.0	0.734 ± 0.005	203 ± 16	0.173 ± 0.005	8.3 ± 0.4	0.093	1.3 ± 0.2	0.34
	25.0	0.829 ± 0.004	238 ± 11	0.108 ± 0.004	8.0 ± 0.4	0.063	1.4 ± 0.2	0.26
	30.0	0.858 ± 0.004	231 ± 11	0.069 ± 0.004	10.6 ± 0.9	0.073	1.9 ± 0.2	0.34
	35.0	0.884 ± 0.003	233 ± 19	0.081 ± 0.004	6.4 ± 0.4	0.035	0.8 ± 0.3	0.49
470	0	0.488 ± 0.006	86 ± 8	0.463 ± 0.008	17.5 ± 0.6	0.049	2.3 ± 0.8	0.25
	4.0	0.613 ± 0.007	82 ± 4	0.278 ± 0.010	13.7 ± 0.8	0.109	2.3 ± 0.4	0.11
	8.0	0.644 ± 0.004	78 ± 3	0.267 ± 0.006	12.5 ± 0.4	0.089	2.4 ± 0.3	0.07
	12.0	0.620 ± 0.005	85 ± 5	0.248 ± 0.008	12.0 ± 0.5	0.132	2.4 ± 0.3	0.10
	15.0	0.535 ± 0.004	94 ± 6	0.403 ± 0.004	16.0 ± 0.4	0.062	2.5 ± 0.3	0.41
	20.0	0.633 ± 0.003	114 ± 5	0.324 ± 0.004	13.9 ± 0.3	0.043	1.5 ± 0.3	0.46
	25.0	0.660 ± 0.003	160 ± 11	0.271 ± 0.004	17.7 ± 0.5	0.069	3.4 ± 0.3	0.44
	30.0	0.728 ± 0.002	168 ± 7	0.218 ± 0.003	15.9 ± 0.4	0.054	2.4 ± 0.2	0.43
	35.0	0.753 ± 0.004	163 ± 9	0.190 ± 0.004	16.5 ± 0.7	0.057	2.8 ± 0.2	0.62

[a] At C_{NaTC} = 0 and 4.0 mM, lifetime data are not available because of low fluorescence intensity.

TABLE 5: Fluorescence Lifetimes (τ) and Fractional Intensity Contributions (f) of Ovalene (2.0 μM) in Aqueous NaTC Solutions at 20 °C (λ_{em} = 470−560 nm)[a]

C_{NaTC}, mM	f_1	τ_1, ns	f_2	τ_2, ns	f_3	τ_3, ns	χ_R^2
4.0	0.045 ± 0.003	71 ± 26	0.225 ± 0.004	3.8 ± 0.1	0.730	0.10 ± 0.01	0.19
8.0	0.059 ± 0.003	56 ± 14	0.296 ± 0.004	4.4 ± 0.1	0.645	0.09 ± 0.01	0.34
12.0	0.099 ± 0.005	86 ± 21	0.346 ± 0.004	4.8 ± 0.1	0.555	0.14 ± 0.02	0.41
15.0	0.106 ± 0.004	68 ± 11	0.441 ± 0.006	4.9 ± 0.1	0.453	0.14 ± 0.02	0.28
20.0	0.130 ± 0.003	65 ± 8	0.434 ± 0.004	5.0 ± 0.1	0.436	0.22 ± 0.02	0.54
25.0	0.159 ± 0.005	87 ± 12	0.438 ± 0.004	5.4 ± 0.1	0.403	0.28 ± 0.03	0.76
30.0	0.150 ± 0.004	108 ± 22	0.458 ± 0.004	5.2 ± 0.1	0.392	0.28 ± 0.03	0.92
35.0	0.165 ± 0.005	124 ± 20	0.480 ± 0.004	5.3 ± 0.1	0.355	0.31 ± 0.03	0.85

[a] At C_{NaTC} = 0 mM, lifetime data are not available because of low fluorescence intensity.

it was necessary to use a single, wide emission window that included both molecular and probe aggregate fluorescence in order to obtain sufficient intensity.

For all probes, the longest-lived fluorescence is attributed to single molecules of probe that are individually solubilized in NaTC aggregates. For pyrene (Table 1), the lifetime of the molecular fluorescence is constant up to 4 mM NaTC and then increases, clearly indicating the initiation of NaTC aggregation and pyrene solubilization at 4 mM. Above 15 mM NaTC, the fractional intensity contribution for the molecular lifetime component remains constant, indicating complete incorporation of pyrene, but the magnitude of the lifetime continues to increase with increasing NaTC. This suggests that the NaTC aggregates are changing as NaTC concentration increases, forming aggregates that are increasingly able to isolate the pyrene molecule in a protected, rigid, hydrophobic binding environment, probably due to increasing aggregate size and internalization of the binding site.

While solubilization of pyrene appears to be complete at 15 mM NaTC, lifetime results indicate that solubilization of BeP and BgP is complete at 20−25 mM and of coronene at 25 mM. Ovalene does not appear to achieve complete solubilization. Pyrene was the only probe that was completely solubilized but did not achieve a plateau for the lifetime of the molecular component, possibly because it has an unusually long lifetime that makes it uniquely sensitive to its microenvironment.

In addition to the long-lifetime components associated with solubilized probe molecules, all of the probes have significantly shorter lifetime components. At least one, and often two, of these components are present at low NaTC concentrations and/

or in pure water. Pyrene has a single short lifetime component (τ_2), probably corresponding to pyrene dimer or excimer, that undergoes a significant lifetime change in the 8−15 mM NaTC region. This lifetime change signals increasing involvement of the NaTC aggregates in the formation of pyrene dimer/excimer, through binding of one or both of the pyrene monomers. Enhanced dimer/excimer formation is indicated as well by the pyrene spectra in Figure 2 in NaTC concentrations of 4 and 8 mM. The further decrease in τ_2 above 20 mM NaTC supports the steady-state fluorescence evidence of this as a critical region.

The case for BeP is similar to that of pyrene in that the shortest lifetime component levels out to a minimum lifetime and fractional intensity at high NaTC concentration (above 20 mM), which again suggests solubilized dimer or excimer. A third component with a somewhat longer lifetime exists in pure water, disappears above 20 mM NaTC, and is probably due to larger probe aggregates in bulk solution.

BgP, coronene, and ovalene have two short-lifetime components at all NaTC concentrations and in pure water (except for ovalene, which could not be measured in pure water). For BgP, the lifetimes and fractional intensities of the components plateau, more or less, between 20 and 25 mM NaTC and are probably due to probe dimer and larger probe aggregates. The changes in lifetime of the components suggest that there are interactions between these probe aggregates and the NaTC aggregates that form above 12 mM NaTC. For coronene, there are no discernible effects of NaTC on the lifetimes of the two short-lifetime components. For ovalene, the lifetimes of the two short-lifetime components tend to increase with increasing NaTC concentration and gradually level off.

Determination of acmc Values Using Average Lifetimes. Various types of average lifetimes, including number-average lifetimes and weight-average lifetimes, have been used in the literature [24,25] to compare heterogeneous lifetimes with each other or with a homogeneous lifetime. To conveniently represent the fluorescence lifetime trends for the different probes in this work, a normalized, average lifetime ($\langle\tau\rangle_{\text{normalized}}$) was calculated for each probe at each NaTC concentration:

$$\langle\tau\rangle_{\text{normalized}} = (\langle\tau\rangle_j - \langle\tau\rangle_{\text{min}})/(\langle\tau\rangle_{\text{max}} - \langle\tau\rangle_{\text{min}})$$

where

$$\langle\tau\rangle_j = \sum_i f_i\tau_i / \sum_i f_i = \sum_i f_i\tau_i$$

The subscript i refers to each of the resolved lifetime components, the subscript j refers to the solution with concentration C_{NaTC_j}, and $\langle\tau\rangle_{\text{max}}$ and $\langle\tau\rangle_{\text{min}}$ are the largest and smallest $\langle\tau\rangle_j$ values of the probe within the NaTC concentration range studied.

Figure 6 shows the plots of normalized average lifetime vs NaTC concentration measured at the molecular peaks (Figure 6a) and aggregate peaks (Figure 6b) of the probes. Ovalene, for which both peaks were included in a single measurement, is included in Figure 6b. Again, all of the probes show the critical region at 8−12 mM. The acmc's indicated in Figure 6 for the probes include 4 mM for pyrene, possibly 4 mM for BeP and coronene, 15 mM for BgP and coronene, and 20 mM for ovalene.

It is interesting that two very distinct transition regions were found for BgP, coronene, and ovalene. For BgP and coronene, the 8−12 mM transition is shown by the molecular peak (Figure 6a) and the acmc at 15 mM is shown by the aggregate peak (Figure 6b). Since the ovalene curve in Figure 6b combines both peaks, both transitions (8 and 20 mM) are shown by the single curve. These results suggest that at least two different

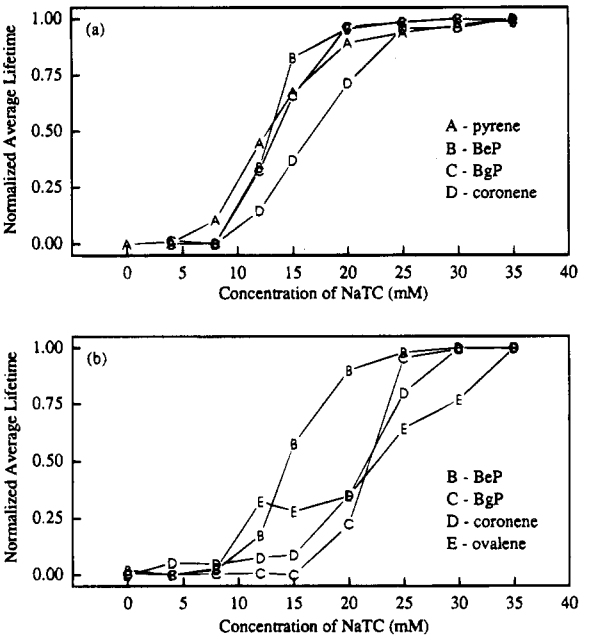

Figure 6. Normalized average lifetimes for the PAH probes in aqueous NaTC solutions, determined from lifetime measurements at (a) a molecular peak and (b) a probe aggregate peak, except for ovalene for which both peaks were included in the broad emission window and are shown in (b).

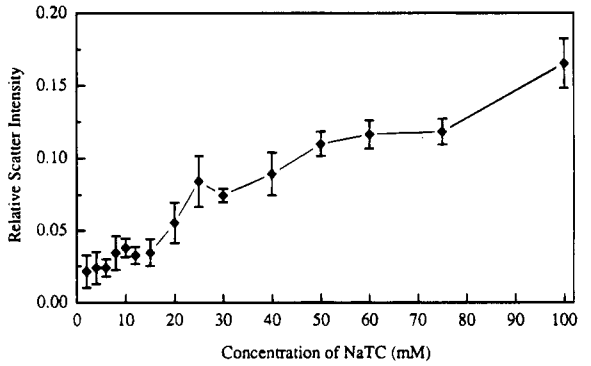

Figure 7. Relative scattered light intensity vs NaTC concentration in the absence of probe. The vertical bars show the standard deviations of the measurements.

forms of NaTC aggregate can participate in the solubilization of these larger probes.

Scattered Light Intensity Results. Relative scattered light intensity vs NaTC concentration in the absence of probe is shown in Figure 7. The curve indicates several critical regions in which transitions to higher intensities occur. These critical regions include 6−8, 15−25, 40−50, and 75−100 mM. The critical region at 40−50 mM was also observed in a fluorescence anisotropy decay study.[16] The transition at 75−100 mM is consistent with results of previous scattered light studies.[2,9]

All of the transition regions are marked by significant increases in scattered light intensity which indicates the formation of larger aggregates or, at higher concentrations, possible phase transitions. It is interesting that these regions tend to immediately precede some of the critical regions seen by the probes, which leads to the conjecture that the formation of the larger aggregates must somewhat precede solubilization of the probes that require the larger aggregates.

Summary of Experimental Results. The cmc is defined as the concentration at which micelles begin to form. In fluorescence probe experiments, the cmc is monitored by changes in the fluorescence properties of a probe upon its solubilization in the micelle. However, if the micellar solution

is polydisperse and probes are used which can sense the formation of different sizes of aggregates, then a broad cmc or even multiple cmcs could be identified. The unique perspective of the polydisperse array of probes used in this work provides a view of increasing aggregate size as NaTC concentration is increased. All of the probes are solubilized to some extent by the aggregates that are formed at the primary critical region of 8−12 mM NaTC, but all of the probes also show at least one acmc, which increase with increasing probe size. Thus, these acmc's must correspond to the formation of aggregates large enough to solubilize particular sizes of probe molecule. Similar critical regions were identified by scattered light intensity measurements in the absence of probe, which confirms that these regions are intrinsic to NaTC and not induced by the probes.

The smallest acmc is around 4 mM, which is consistent with previous work[10,11] and is attributed to the formation of dimer.[16] Only the smaller probes report this transition region. The so-called quasi-cmc[11] at 8−12 mM NaTC was detected by all of the probes, indicating that a larger NaTC aggregate is formed at this concentration that can solubilize all of the probes to some extent. This is consistent with previous work in which larger NaTC aggregates, such as tetramer, were suggested to form at the quasi-cmc.[1,2,16] The two largest acmc's at 15 and 20 mM were detected by the three largest PAH probes. These acmc's are higher than the commonly accepted cmc's for bile salts, although critical regions around 20 mM have been previously reported for NaC[13,26] and NaTC.[16] They correspond to the formation of even larger aggregates (>tetramer).

Molecular Modeling Studies. The experimentally observed acmc's should correspond to the formation of increasingly larger NaTC aggregates that can solubilize increasingly larger probes. Using molecular modeling methods, it is possible to estimate the sizes of the NaTC aggregates and propose reasonable structures for the probe−NaTC complexes that are formed at the various acmcs.

Based on an empirical theory in which the lowest free energy conformation of a molecular system minimizes the exposure of a hydrophobic surface to the aqueous phase, a criterion was set for a solubilized PAH probe: the solubilized probe should have its aromatic ring surface protected as much as possible from the bulk aqueous solution. Additionally, the smallest NaTC aggregate able to solubilize a given PAH probe is assumed to form at the first cmc detected by the probe.

The dimensions of the PAH probes and the NaTC monomer are shown in Figure 1. The smallest aggregate able to solubilize a probe is the dimer, to form a "sandwich dimer" as previously described for perylene in NaTC.[16] Figure 8a shows that when pyrene is sandwiched between two NaTC monomers, its aromatic ring surface is just covered by the two monomers. The three methyl groups and the hydrogen atoms on the hydrophobic surface of the NaTC molecule are involved in the hydrophobic interaction with the probe. Therefore, the NaTC molecule is tilted to provide maximum contact with the pyrene molecule. The hydrophilic tail of NaTC does not appear to contribute to the aggregation since the two tails remain apart in the dimer and their conformation in the optimized dimer does not change significantly from their conformation in the monomer.

The formation of dimers is assigned to the lowest acmc at 4 mM, which is detected by pyrene. This is consistent with the suggestion of previous work.[16] For larger probes, the dimer cannot fully cover the aromatic ring surface, leaving the probes to protrude into the aqueous phase if solubilized in the dimer as previously suggested for BeP and BgP.[23] It is interesting that the dimer covers BeP no better than BgP although BgP is larger by one ring. This may be due to the effects of shape in addition to size (see Figure 1). The dimer is clearly too small to effectively solubilize the large coronene and ovalene probes.

The NaTC tetramers match the sizes of the two larger probes studied. In the molecular mechanics calculation, two different optimum conformations were obtained for tetramer−probe complexes. One ovalene−tetramer model (Figure 8b) is actually an analog to the sandwich dimer model (Figure 8a) but with ovalene sandwiched in four monomers (two on each side). In the conformation shown in Figure 8b, the hydrophilic tails are involved in intraaggregate molecular interactions, and consequently the total energy is lowered by an extra ~10 kcal/mol. However, solvent is not included in these calculations and would tend to lower the effects of tail interactions.

The other ovalene−tetramer conformation (Figure 8c) forms in a different way: two hydrophobically bonded dimers sandwich the probe within their hydrophobic surfaces. The energy difference between the two tetramer conformations is within thermal energy ($\sim kT$). Therefore, the tetramer is proposed as the aggregate that is responsible for the primary critical region 8−12 mM, detected by all five probes, because the tetramer can cover the surfaces of all of the probes. This is consistent with previous reports of tetramer formation at the critical region of 8−12 mM.[1−4]

BgP and coronene both detect the same acmc at 15 mM due to their similar size, but the solubilization processes are different: the BgP aggregate peak disappears by 35 mM NaTC but the coronene aggregate peak stays. This indicates that the stability of the probe aggregates are different. From another point of view, this also suggests that the existence of the equilibrium of PAHs in different forms does not affect the acmc detection. The acmc indicated by BgP and coronene at 15 mM is most likely due to hexamer formation.

The ovalene−octamer model (Figure 8d) has strong hydrophobic interactions among its components: ovalene is well isolated from the bulk solution and the hydrophobic surfaces of the NaTC monomers are internalized to protect them from the bulk solution. The acmc of ovalene at 20 mM is therefore attributed to octamer formation.

In some of the above models, there is room to fit more NaTC monomers on the sides of the aggregates to form larger aggregates such as decamers and dodecamers, but they may not be necessary for solubilization of the probes and are therefore not identified by an acmc. Also, aggregates with even numbers of monomers are more likely to be sensed by the PAH probes due to their planar symmetry.

In summary, the model for the probe−NaTC complexes indicated by the fluorescent probes and supported by molecular modeling includes initial formation of dimers at 4 mM, tetramers at 8−12 mM, hexamers at 15 mM, and octamers at 20 mM. Furthermore, the range of aggregate sizes involved in solubilization is indicated at concentrations up to 20 mM.

NaTC Aggregates in the Presence and Absence of PAH Probes. According to the original and modified primary−secondary micelle models,[1,5,6] dimers, tetramers, octamers, and dodecamers are all possible primary aggregates and secondary micelles are formed by hydrogen bonding between primary micelles. This model was based on an early molecular modeling study which proposed the formation of primary, hydrophobically bonded micelles containing up to 10 bile salt monomers.[5] Compared with dihydroxy bile salts, trihydroxy bile salts such as NaTC form smaller aggregates in aqueous solution, the majority of which are primary micelles.[1−6] The driving force for formation of primary aggregates is hydrophobic attraction whether or not PAH probes are involved.

None of the PAH probes shows any evidence of inducing aggregation, as evidenced by the absence of solubilization below

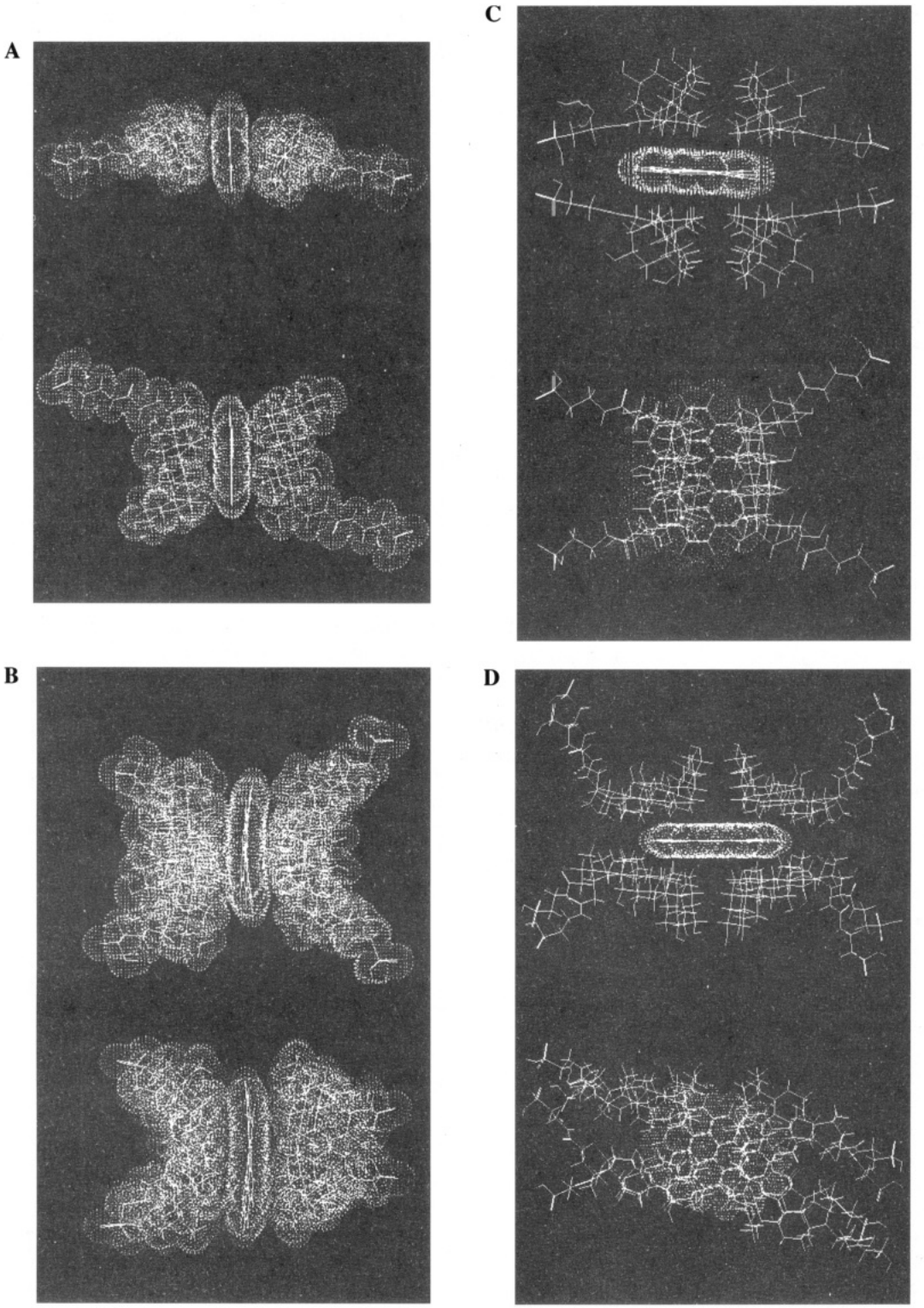

Figure 8. Models for the solubilization of pyrene and ovalene in primary NaTC micelles. All figures show the optimal conformations obtained from molecular modeling calculations. (A) Sandwich model for pyrene solubilized in a NaTC dimer; (B) and (C) sandwich models for ovalene solubilized in NaTC tetramers; (D) model for ovalene solubilized in a NaTC octamer.

the first acmc at 4 mM, nor do they affect the critical concentrations in NaTC aggregation since the same critical regions are observed using scattered light measurements in the absence of probe. Moreover, smaller PAH probes are not expected to significantly perturb the aggregate structures since the models show that they fit easily into the existing solubilization sites in the aggregates. However, for large PAHs like coronene and ovalene, the situation may be more complicated. Although the larger PAH probes do not appear to significantly affect the critical regions, they may cause distortions in the aggregate shapes. Moreover, a particular aggregate conformation may predominate in the solubilization of a probe among "isomers" with the same aggregation number if its shape is particularly suited to incorporation of the probe. In fact, as discussed in the following section, some possible aggregate conformations do not provide sufficient room for probes, especially the larger probes.

Model for NaTC Aggregation and Probe Solubilization. On the basis of the experimental results and the molecular modeling studies, we propose a model for NaTC aggregation and probe solubilization in solutions containing up to 35 mM NaTC. Previously proposed models, including the primary–

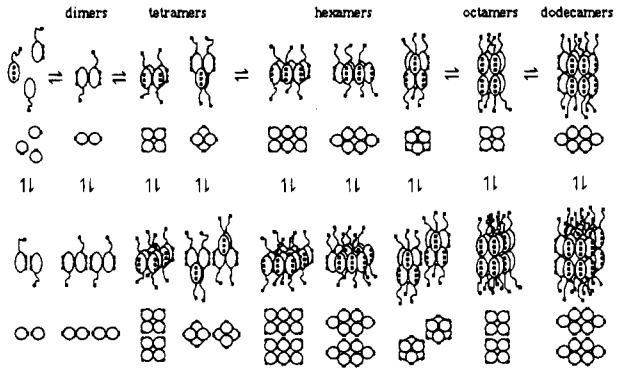

Figure 9. Aggregation model for NaTC micelles. Different views of the aggregates are shown. The black squares are the hydroxyl groups on the NaTC monomers.

secondary model,[5] the modified primary−secondary model,[6] and hydrogen bonding model,[7] were all considered in the formulation of the proposed model. The model is illustrated in Figure 9, in which the bile salt monomer is represented as a prolate, ellipsoidal body with a flexible hydrophilic tail and the three black dots on the rigid body are the hydroxyl groups. For each aggregation number, all isomeric aggregate forms are shown that were determined by molecular mechanics calculations to be optimal. The largest aggregate that can be formed solely through hydrophobic interaction is taken to be the dodecamer.[6] All of the aggregate structures tend to maximize the van der Waals contact between monomers. For instance, the two primary tetramers in Figure 9 have different minimum energies: the aggregate on the left in which hydrophobic interactions are maximized is >10 kcal/mol more stable than the aggregate on the right, in the absence of effects of solvent.

Secondary micellization through hydrogen bonding may actually be more complicated than what is proposed in Figure 9 since the three hydroxyl groups are not located in the same plane that is parallel to the body. Before looking at secondary micelles, it is interesting to consider the hydrogen-bonded dimer. In this case only two identical pairs of hydrogen bonds (between $C_{(3)}OH$ and $C_{(12)}OH$) are indicated by the molecular mechanics calculation (the distance between O and H: $d_{O,H} = 2.2$ Å) and an interior cavity may allow inclusion of at least one water molecule. The third hydroxyl group ($C_{(7)}OH$) in both monomers in the dimer has a weak hydrogen-bonding interaction ($d_{O,H} =$ 2.6 Å) and is accessible to water. An NMR study of NaC showed that a change in the chemical shift of the hydroxyl carbons as function of NaC concentration is slightly different for $C_{(7)}$ relative to $C_{(3)}$ and $C_{(12)}$.[24] Also, the hydrogen-bonded dimer is only ~3.5 kcal/mol more stable than the hydrophobically bonded dimer, which is close to the thermal energy of the solution. Therefore, if solvent molecules were included in the computation, formation of the hydrogen-bonded dimer would probably be less favorable due to competition from water for hydrogen bonding as well as the unfavorable contact between the hydrophobic surface of the bile salt and the aqueous solvent.

In the case of secondary tetramer formation through hydrogen bonding of two primary, hydrophobically bonded dimers, the unfavorable contact is still a competing driving force leading to the formation of primary tetramers, since some of the hydrophobic surfaces are exposed to the aqueous phase in the secondary tetramer. In the absence of water, the primary tetramer is energetically favored over the secondary tetramer by ~10 kcal/mol. This would suggest that hydrophobic interactions are more important than hydrogen bonding in the formation of larger aggregates, at least until all of the hydrophobic NaTC surfaces in the aggregate are in the micellar interior and isolated from the bulk solution.

For trihydroxy bile salts, small aggregates form in aqueous solution and most of the aggregates are believed to be primary micelles .[1-6,16] Although hydrogen-bonded models for dimerization[7] and primary−secondary micellization[5,6] were both proposed for trihydroxy bile salts, hydrogen bonding does not appear to be an important factor energetically in the formation of NaTC aggregates as large as dodecamers under the conditions used in these studies. If many pairs of NaTC monomers are involved in the hydrogen bonding between primary aggregates or if the hydrophilic tails are involved, then secondary micelles might form between smaller, primary aggregates. Further studies are needed, however, before the role of hydrogen bonding in the aggregation of NaTC in water can be fully understood.

Acknowledgment. This work was supported by the Division of Chemical Sciences, Office of Basic Energy Sciences, Office of Energy Research, United States Department of Energy (Grant Number DE-FG0588ER13931) and by the Environmental Protection Agency (Grant R817127-01). The authors are grateful to Dr. John C. Fetzer in Chevron Research Center for providing the ovalene used in this work.

References and Notes

(1) Small, D. M. In *The Bile Acids*, Nair, P. P., Kritchevsky, D., Eds., Plenum Press: New York, 1971; Vol. 1, Chapter 8.
(2) O'Connor, C. J.; Wallace, R. G. *Adv. Colloid Interface Sci.* **1985**, *22*, 1.
(3) Setchell, D. R., Kritchevsky, D. and Nair, P. P. *The Bile Acids*; Plenum Press: New York, 1988; Vol. 4.
(4) McGown, L. B.; Meyerhoffer, S. M.; Hertz, P. R.; Li, G. Luminescence Measurements in Bile Salt Micelles. In *Analytical Chemistry in Organized Media;* Hinze, W. L., Ed.; JAI Press: Greenwich, CT; Vol. 2, in press.
(5) Small, D. M. *Adv. Chem. Ser.* **1968**, *84*, 31.
(6) Mazer, N. A.; Carey, M. C.; Kwasnick, R. F.; Benedek, G. B. *Biochemistry* **1979**, *18*, 3064.
(7) Oakenfull, D. G.; Fisher, L. R. *J. Phys. Chem.* **1977**, *81*, 1838.
(8) Campanelli, A. R.; Candeloro De Sanctis, S.; Chiessi, E.; D'Alagni, M.; Giglio, E.; Scaramuzza, L. *J. Phys. Chem.* **1989**, *93*, 1536.
(9) Fontell, K. *Kolloid-Z. Z. Polym.* **1971**, *244*, 253.
(10) Hashimoto, S.; Thomas, J. K. *J. Colloid Interface Sci.* **1984**, *102*, 152.
(11) Meyerhoffer, S. M.; McGown, L. B. *Langmuir* **1990**, *6*, 187.
(12) Kratohvil, J. P.; Hsu, W. P.; Jacobs, M. A.; Aminabhavi, T. M.; Mukunoki, Y. *Colloid Polym. Sci.* **1983**, *261*, 781.
(13) Mukerjee, P.; Cardinal, J. R. *J. Pharmacol. Sci.* **1976**, *65*, 882.
(14) Ruckenstein, E.; Nagarajan, R. *J. Phys. Chem.* **1975**, *79*, 2622.
(15) Moroi, Y. *J. Colloid. Interface. Sci.* **1991**, *141*, 581.
(16) Li, G.; McGown, L. B. *J. Phys. Chem.* **1993**, *97*, 6745.
(17) Waris, R.; Rembert, M. A.; Sellers, D. M.; Acree Jr., W. E.; Street, K. W., Jr.; Poole, C. F.; Shetty, P. H.; Fetzer, J. C. *Appl. Spectrosc.* **1988**, *42*, 1525.
(18) MacKay, D.; Shiu, W. Y. *J. Chem. Eng. Data* **1977**, *22*, 399.
(19) Nakajima, A. *Photochem. Photophys.* **1977**, *25*, 593.
(20) Weinberger, R.; Cline Love, L. J. *Spectrochem. Acta* **1984**, *40A*, 49.
(21) Kalyanasundaram, K. In *Photochemistry in Organized and Constrained Media*, Ramamurthy, V., Ed.; VCH: New York, 1991; Chapter 2.
(22) Kalyanasundaram, K.; Thomas, J. K. *J. Am. Chem. Soc.* **1977**, *99*, 2039.
(23) Meyerhoffer, S. M.; McGown, L. B. *Anal. Chem.* **1991**, *63*, 2082.
(24) Tran, C. D.; Fendler, J. H. *J. Phys. Chem.* **1984**, *88*, 2167.
(25) Bauer, R. K.; de Mayo, P.; Ware, W. R.; Wu, K. C. *J. Phys. Chem.* **1982**, *86*, 3781.
(26) Campredon, M.; Quiroa, V.; Thevand, A.; Allouche, A.; Pouzard, G. *Magn. Res. Chem.* **1986**, *24*, 624.
(27) Funasaki, N.; Hada, S.; Neya, S. *J. Phys. Chem.* **1991**, *95*, 1846.

JP9421491